Journal of Building Engineering 108 (2025) 112890

Contents lists available at ScienceDirect

Journal of Building Engineering

journal homepage: www.elsevier.com/locate/jobe

Masonry retrofitting with steel reinforced plaster: experimental and analytical study

Manuela Scamardo *, Sara Cattaneo, Pietro Crespi

Politecnico di Milano, ABC Department, Milano, Italy

ARTICLE INFO

Keywords:
Masonry
Overlay retrofitting system
Steel reinforced plaster
Diagonal compression test

ABSTRACT

This paper presents the results of an experimental program aimed at assessing the effectiveness of steel reinforced plaster in improving the performance of masonry walls under cyclic loads, analysing the effect of the main design parameters. Diagonal compression tests were performed under displacement control. Unreinforced specimens were also tested as reference. The investigated parameters were: the masonry thickness (250 or 380 mm), the overlay thicknesses (30 or 50 mm), the type of mortar used for the overlay (cementitious or lime-based), and the number of connectors (8 or 12 for each side of the specimen). An analytical approach, previously presented by the authors, is recalled and further validated using the new experimental data, and a parametric study is performed to better discuss the effect of some design parameters. The results show that the load capacity of specimens retrofitted with lime-based plaster resulted at least equivalent to the one retrofitted using the most common cementitious one, and in some cases superior, with higher displacement at the ultimate load. Higher overlay thickness has a positive effect in terms of post-peak ductility for the cementitious plaster, and higher load bearing capacity for the lime plaster. An increasing number of connectors does not affect the ultimate load but results in a late detachment of the plaster layers. The analytical method results still valid by considering the new presented experimental data. The parametric study confirms that the strength and thickness of the overlay are crucial for the load bearing capacity of the specimen, while the number of connectors does not affect significantly the ultimate load.

1. Introduction

Unreinforced masonry structures were usually built in the past under empirical rules to resist only to vertical loading. For this reason, most of them result vulnerable to lateral loads such as that imposed by earthquakes [1–3], requiring strengthening interventions to guarantee the structural safety and limit the economic and human losses after seismic events.

In the last few decades, different retrofitting techniques have been developed and implemented to improve the behaviour of masonry buildings under seismic actions [4–6], using more conventional approaches (e.g. shotcrete, grout injections) [7,8] or introducing innovative materials and techniques (e.g., fiber-reinforced polymers grid or strips) [9–12]. The choice of the most appropriate retrofitting method should be made by carefully considering several factors: (i) cost, (ii) sustainability, (iii) compatibility, (iv) durability and, in case of historical heritage structures, (v) reversibility and (vi) minimum intervention. Stitching and grout injections into the walls are often used to fill voids or cracks and restore the masonry initial strength, with minimal cost, availability of

* Corresponding author.
E-mail address: manuela.scamardo@polimi.it (M. Scamardo).

https://doi.org/10.1016/j.jobe.2025.112890
Received 6 March 2025; Received in revised form 26 April 2025; Accepted 8 May 2025
Available online 9 May 2025

material and ease of application without requiring much technical rigor [13]. Repointing is adopted when bricks are of good quality but the mortar is poor. This last one is replaced using higher strength materials, including fiber or textile reinforced mortar or steel reinforced grout [14]. External reinforcements are quite common to improve the masonry in-plane and out-of-plane behavior and consist in installing reinforcing elements next to a structure to carry external loads and to control the propagation of cracks. They can include, for instance, fiber-reinforced polymers grid or strips [15], steel systems [16] or more sustainable materials as bamboo stems [17]. Surface treatment involves the realization of a steel or polymer mesh around the wall to be coated with a layer of mortar [18,19]. In seismic prone areas, the use of overlays to retrofit existing masonry buildings is a common practice due to the limited costs and the effectiveness of the method in improving the strength, stiffness, and deformation capacity of the masonry structure, both in-plane and out-of-plane. However, one main drawback of this approach is the increase of the dead weight of the strengthened elements, that should be carefully controlled. Furthermore, as masonry overlays completely cover the masonry walls, their application in buildings with architectural and historical value is often not permitted.

Overlays can include different types of reinforcement such as steel, polymers, and carbon or glass fibers to enhance their tensile strength [20–25]. To avoid the use of reinforcement, cementitious composites reinforced with synthetic fibers are sometimes adopted [26,27]. One of the most common and traditional overlay applications is the steel reinforced plaster (SRP). It usually consists in layers of plaster made by cementitious mortar or concrete, reinforced using steel meshes. The plaster thickness commonly ranges between 30 and 70 mm. Steel anchors are usually introduced into the masonry and connected to the steel mesh to transfer the shear stresses across the concrete-masonry interfaces and avoid buckling phenomena. In job sites, this traditional SRP approach is often preferred with respect to other innovative materials and techniques thanks to its limited costs, easy application and no need of high skilled manpower. Furthermore, the method is recommended as an effective retrofitting technique by several Design Codes [28–31]. Recently, applications of SRP with lime-based mortar have been introduced, with several benefits such as superior compatibility with the masonry substrate, transpirability (which avoids moisture problems), and higher sustainability with respect to the cement one [32,33]. Indeed, lime mortar is a natural carbon-neutral building material while the cement production is a highly energy-intensive process that releases a lot of greenhouse gases into the atmosphere.

Despite SRPs are commonly adopted in practice, the scientific literature on the topic is rather limited. Ghiassi et al. [34] studied the behavior of masonry walls strengthened with reinforced concrete layers only from a numerical perspective with the aim of developing an analytical method to predict the response of the retrofitted walls. Churilov et al. [35] experimentally investigated the performance under cyclic horizontal load of masonry walls strengthened by applying reinforced concrete jackets on both sides, finding a significant improvement of the shear resistance in the retrofitted specimens with respect to the unreinforced ones. Gattesco et al. [36] presented the results of an experimental program conducted on several typology of masonry walls strengthened with mortar coating reinforced with GFRP meshes or steel mesh to evidence the effectiveness of the applied strengthening technique. Maddaloni [37] presented the study of tuff masonry specimens retrofitted with GFRP meshes or steel mesh, considering different type of mortar for the overlay.

The purpose of the presented research is to improve the knowledge on SRP technique, studying the effect of several design parameters on the structural response. A broad experimental investigation was conducted considering unreinforced and SRP-retrofitted masonry specimens subjected to diagonal compression tests under cyclic loads. The tests configurations considered different masonry thicknesses, plaster thicknesses, types of mortar used for the plaster overlay, number of anchors used to connect the steel mesh to the masonry. The first part of the experimental research, related to the application of SRP made with cementitious mortar overlay, has been already published [38]. This paper presents instead the whole research results, analysing and discussing in detail the main outcomes. The analytical method proposed in Ref. [39] is than recalled and used to perform a parametric study to better examine the effect of some design parameters.

2. Experimental research

2.1. Specimens and materials

The experimental program considers a total of 14 specimens, 4 unreinforced and 10 retrofitted changing different design

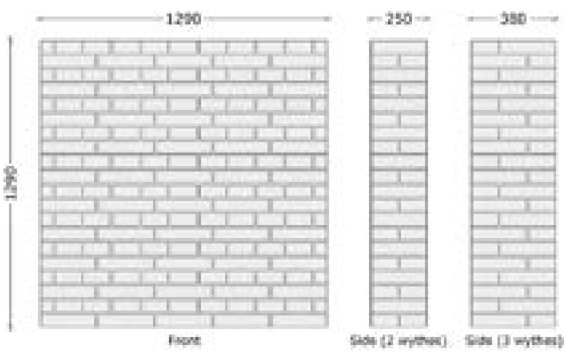

Fig. 1. Geometry of unreinforced masonry specimen.

parameters. The unreinforced specimens had dimensions of 1290 × 1290 mm and thickness of 250 mm (2 whytes) or 380 mm (3 whytes) (Fig. 1). The walls were built according to the English bond rule using solid clay bricks with dimension of 250 × 120 × 55 mm and a lime mortar (1:5 water/cement ratio by weight) classified as M2.5 according to Eurocode 6 [40] to fill the joints, having 10 mm thickness. The average compressive strength of the bricks obtained from uni-axial compression tests [41] was 23.3 MPa (cov 5.5 %). The mean value of mortar compressive strength evaluated according to Ref. [42] was 5.4 MPa (cov 13.5 %).

In the strengthened configurations, a layer of steel reinforced plaster was applied on each side of the specimen. A steel mesh of 6 mm diameter wire (B450C class), with a spacing of 100 mm in both horizontal and vertical directions, was used as reinforcement. Steel anchors in the form of steel ribbed rebars (B450C, 8 mm diameter), bent at one end with a 90-degree hook of length 50 mm, were used to connect the plaster layer to the masonry. The anchors were installed in pre-drilled holes of 10 mm diameter and 200 mm of embedment depth, filled with the Hilti HIT-HY 270 injection mortar. Different design parameters were experimentally investigated: (i) the overlay material type, considering as plaster a cement-based mortar or a lime-based one; (ii) the overlay thickness, 30 or 50 mm; (iii) the number of connectors, 8 or 12 according to the layouts reported in Fig. 2. The plaster mechanical properties were evaluated with uniaxial compressive tests and three point bending tests according to Refs. [42,43]. The cement-based plaster was a ready-mix mortar with average compressive strength of 33.8 MPa (cov 3.80 %) and an average flexural strength of 6.38 MPa (cov 13.38 %). The lime-based plaster was also a ready-mix mortar with average compressive strength of 18.9 MPa (cov 3.14 %) and an average flexural strength of 4.76 MPa (cov 7.91 %). During the curing time of the mortar coatings (at least 28 days), the wall surfaces were covered with a wet blanket to avoid shrinkage cracks.

A summary of the performed tests with the main specimen properties is reported in Table 1. For each configuration, the number of repetitions, and the identification code (M: masonry, U/R: unreinforced or retrofitted, number of wythes (2 or 3), thickness of the plaster in cm, number of anchors, C/L cementitious or lime mortar) are also reported. The experimental program was performed in two different subsequent campaigns: in the first one, the unreinforced specimens and the ones retrofitted with cementitious plaster were tested [38]; in the second set of tests, the specimens retrofitted with lime-based plaster were tested. Since the coefficient of variation for the retrofitted specimens of the first set was very low (about 3 %), in the second set of tests only one specimen for each configuration was tested.

2.2. Test set-up and procedure

The masonry specimens were tested under diagonal compression tests according to the ASTM E519 Standard [44]. Two hydraulic jacks, with capacity of 300 kN each, were placed diagonally on both sides of the specimen (Fig. 3a and b) to apply the load. The load was continuously monitored by two load cells with capacity of 300 kN each. The displacement applied by the hydraulic jacks was transferred to the wall corners using two L-shaped steel shoes.

The tests were performed under displacement control. The displacement along the diagonals was monitored using linear variable differential transformers (LVDTs) with gauge length of about 800 mm, two for each side of the wall. For the strengthened specimens, two additional LVDTs per side was placed orthogonally to the wall front/back face to monitor the out-of-plane deformation. The LVDTs layout is shown in Fig. 3c.

The displacement was applied according to the protocol proposed by Porter [45] which considers two main phases: (i) application of monotonic load until the first main crack is detected, i.e., first major event (FME); (ii) application of cyclic displacement history, defined on the basis of the displacement associated to the FME. The first 10 increasing cycles are defined as the 25 % (3 cycles), 50 % (3 cycles) and 75 % (3 cycles) of the FME displacement, plus a final cycle at 100 %. The unloading is then performed with 3 decreasing cycles. The displacement is then stabilized by applying 3 cycles at 100 %. If the load decrease between two successive cycles is less than 5 %, the system is considered stable. The protocol proceeds with one cycle at 125 % FME, 3 progressive unloading cycles and 3 stabilizing cycles at 125 % FME. The sequence is then repeated by increasing each time the target FME percentage by 25 %. The displacement protocol is reported in Fig. 4.

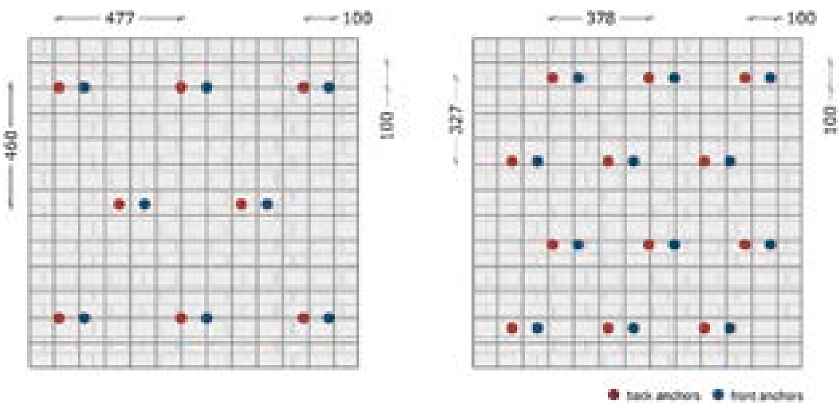

Fig. 2. Reinforcement configuration with 8 (left) and 12 (right) anchors.

Table 1
Test program, code and specimen characteristics.

Code	Wall			Reinforced plaster			#repeats
	Width (mm)	Height (mm)	Thickness (mm)	Thickness (mm)	Mortar type	#anchors	
MU2	1290	1290	250	–	–	–	2
MU3			380	–	–	–	2
MR2-3-8-C			250	30	Cem	8	2
MR2-5-8-C			250	50	Cem	8	2
MR3-5-8-C			380	50	Cem	8	2
MR2-3-8-L			250	30	Lime	8	1
MR2-3-12-L			250	30	Lime	12	1
MR2-5-8-L			250	50	Lime	8	1
MR2-5-12-L			250	50	Lime	12	1

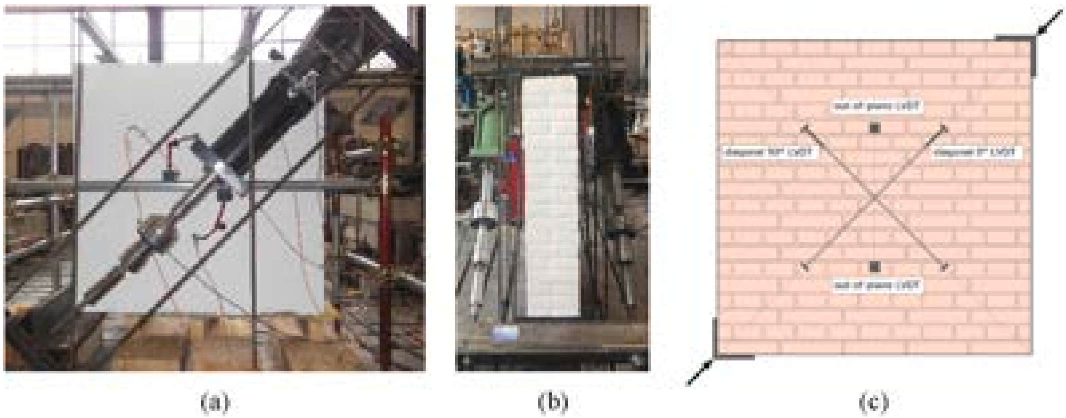

Fig. 3. Test set-up: (a) front view, (b) side view and (c) LVDT's layout.

It should be underlined that, due to damage developed during cycles, it was not always possible to reach the original jack position with the consequent recording of residual stroke after a certain displacement level.

2.3. Test results

The main results of the experimental tests are summarized in Table 2. In particular, the load and the stroke (displacement of the jacks) associated to the FME, to the peak (ultimate load), and to the final failure (residual load) of the specimen are reported, together with the percentage of FME at the peak and at the final failure and the area of the hysteresis loops. The ultimate and residual loads are also plotted in Fig. 5 vs. the strain (a, b) and the stroke (c, d) for cementitious and lime plaster specimens. The stroke associated to the FME in the tests with lime plaster was assumed equal to 6.58 mm on the basis of the mean FME strokes recorded for the unreinforced specimens and the ones with cementitious plaster.

In general, in terms of ultimate load, the lime-based plaster was able to reach the capacity of the cementitious plaster, and, in some cases, also to overcome it. For instance, considering the analogous specimens MR2-5-8-L vs. MR2-5-8-C, an increase of the load of

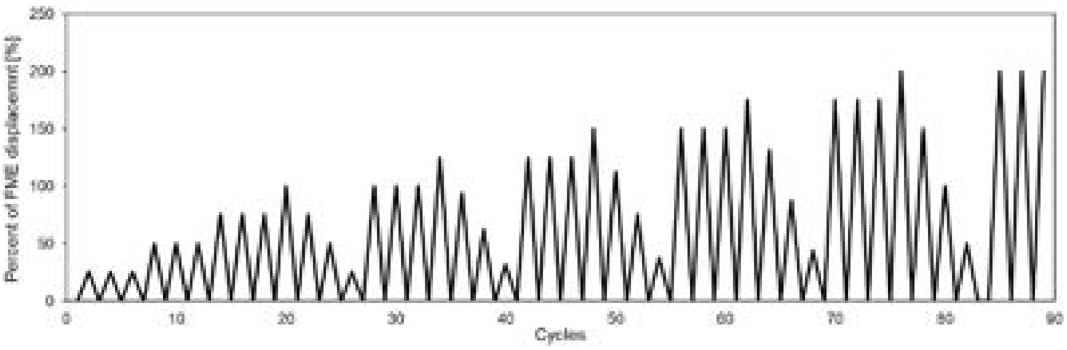

Fig. 4. Cyclic SPD protocol.

Table 2
Test results.

Code	FME		Maximum load			Residual load			Area of hysteresis loop
	Load	Stroke	Load	Stroke	%FME	Load	Stroke	%FME	
	kN	mm	kN	mm	–	kN	mm	–	kNmm
MU2-1	199.13	6.58	232.22	7.48	114 %	–	–	–	733.9
MU2-2	–	–	165.12	5.69	87 %	–	–	–	519.5
MU3-1	252.79	6.24	451.07	11.11	178 %	–	–	–	2563.7
MU3-2	–	–	229.69	7.35	118 %	–	–	–	795.3
MR2-3-8-C-1	202.54	5.69	366.80	12.64	222 %	112.46	21.43	377 %	3890.1
MR2-3-8-C-2	–	–	372.45	13.32	234 %	157.98	31.06	546 %	5720.1
MR2-5-8-C-1	277.17	8.17	376.63	11.69	143 %	208.53	38.50	471 %	7247.2
MR2-5-8-C-2	–	–	373.97	13.14	161 %	164.24	44.51	545 %	7735.7
MR3-5-8-C-1	241.10	8.25	539.13	18.87	229 %	209.13	44.82	543 %	9804.03
MR3-5-8-C-2	–	–	565.27	17.10	207 %	180.59	45.00	545 %	10749.8
MR2-3-8-L	–	–	363.25	27.75	422 %	94.70	38.04	579 %	5409.7
MR2-3-12-L	–	–	344.14	18.98	289 %	215.78	45.60	693 %	7536.2
MR2-5-8-L	–	–	497.84	19.11	291 %	165.86	26.48	403 %	6935.8
MR2-5-12-L	–	–	509.37	22.08	336 %	199.72	29.46	448 %	7414.2

about 25 % was recorded with respect to the cementitious plaster. The residual load and areas of the hysteresis loop resulted comparable. The stroke resulted instead always higher in the case of the lime plaster (range 18.98–27.75 mm) with respect to the cement-based one (range 11.69–13.32 mm).

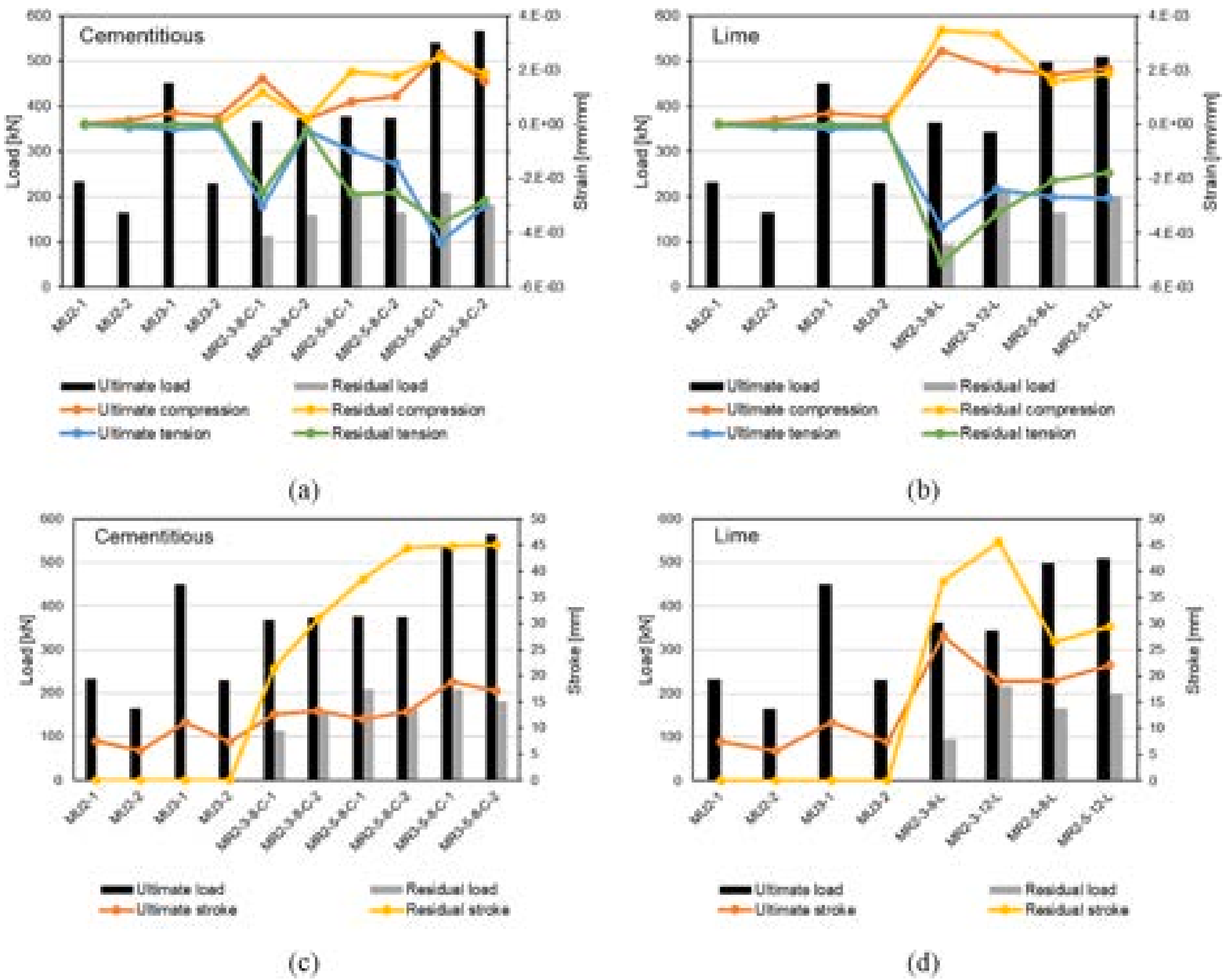

Fig. 5. Ultimate/residual loads vs. strain (a,b) and vs. stroke (c,d) for cementitious and lime plasters specimens.

3. Discussion

In order to better understand the influence of the investigated design parameters, several comparisons in terms of load vs. displacement curves are reported in the following sections. The curves of the unreinforced configurations are always reported as reference.

It should be highlighted that the limited number of repetitions for the different layout configurations does not allow to make relevant statistical considerations on the results. However, the obtained coefficient of variation was quite low for the retrofitted specimens (0.5 %–3.3 %), while it was much greater for the unreinforced ones (23.9 %–46 %). This was probably due to the fact that the heterogeneity of masonry and the presence of weak regions in the specimens can cause significant variations of the response, in terms of peak load and detected damage, while the introduction of homogeneous layers of plaster can provide a stabilizing effect in the fracture process.

3.1. *Effect of the masonry thickness*

Fig. 6 shows the load vs. displacement curves of unreinforced and retrofitted specimens with different masonry thickness, i.e. 250 cm (MU2 and MR2) and 380 cm (MU3 and MR3), considering a cementitious plaster with thickness of 5 cm.

In general, both in case of unreinforced and retrofitted walls, the failure mode and the stiffness of analogous specimens with different masonry thicknesses were constant. In particular, the unreinforced specimens (MU2-1 and MU3-1) exhibited brittle failure with a limited number of cycles whatever the masonry thickness, while reinforced specimens (MR2-3-8-C-1 and MR3-5-8-C-1) underwent to a large number of cycles (up to 100), which resulted in a high area of hysteresis loops. The influence of the masonry thickness was instead evident in terms of deformation or load capacity: indeed, higher wall thickness increased both the deformation and load capacity.

3.2. *Effect of the plaster thickness*

Fig. 7 shows the load vs. displacement curves of unreinforced and retrofitted specimens with different plaster thickness, i.e. 3 cm and 5 cm, considering cementitious (left) or lime (right) plaster.

In case of cementitious plaster, no significant difference was detected in terms of bearing capacity by changing the plaster thickness from 3 to 5 cm, even if the ductility of the specimen improved considerably. This phenomenon could be explained considering that the plaster layers were subjected to a complex state of axial force and bending with shear stresses in the non-delaminated masonry-plaster contact areas. These shear stresses appeared to have a greater influence on the bending of the thicker plaster layers which results in an increased ductility of the masonry wall reinforced with thicker plaster layers. On the contrary, in case of lime plaster, the increase of plaster thickness resulted in an increase of the ultimate load, with similar dissipation capacity. Moreover, in both cases (cementitious and lime), the final residual strength (obtained by increasing monotonically the displacement at the end of the test until failure) increased by increasing the thickness of the plaster (Table 2).

In general, it was evident that the higher plaster thickness had positive effects in terms of higher post-peak ductility for the cementitious plaster, and higher load bearing capacity in the case of the lime plaster.

The damage detected on the specimens after the tests for different plaster thickness (and same other design parameters) resulted similar (Fig. 8). Multiple diagonal cracks were observed in the direction of the application of the load, together with crushing in the loaded corners, and the punching of the plaster due to the anchors bending that was more evident in case of lower thickness. However, by looking at the ultrasonic measurements of Fig. 9, it is evident that, both in case of lime (a,b) or cementitious (c,d) plaster, the thicker layer of coating (5 cm) is affected by a earlier damage and detachment from the masonry substrate with respect to the thinner one (3 cm). Indeed, at the same level of imposed displacement, the damage area is always more extended and the detachment clearly evident (dark areas where the measurement cannot be acquired because of the detachment). This suggests that excessively thick coatings may

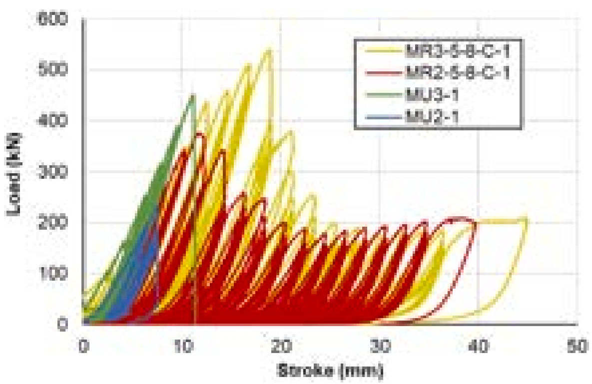

Fig. 6. Load vs. displacement curves for specimens with different masonry thickness.

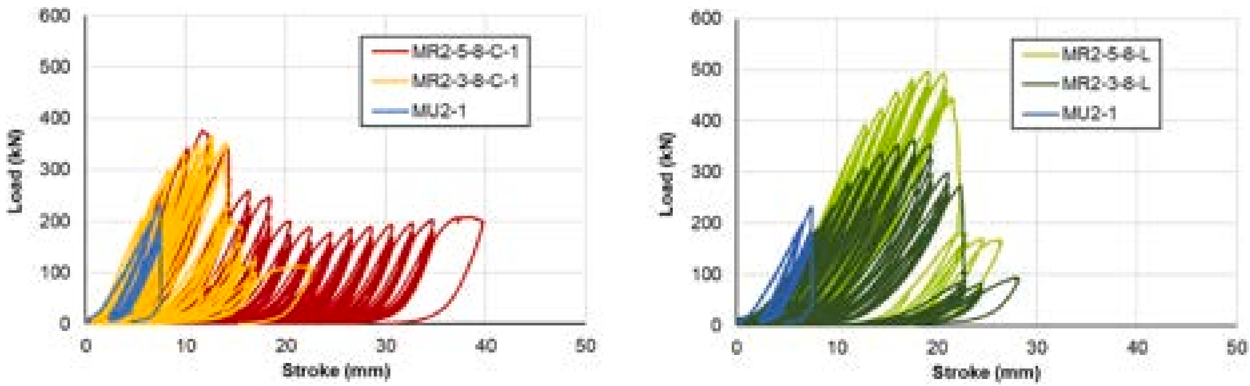

Fig. 7. Load vs. displacement curves for specimens with different plaster thickness: left, cementitious plaster with 3 or 5 cm of plaster thickness, right lime plaster with 3 or 5 cm of plaster thickness.

not always proportionally enhance the performance and could introduce risk of cracking and new failure mechanisms.

3.3. Effect of the type of plaster overlay

Fig. 10 shows the load vs. displacement curves of unreinforced and retrofitted specimens with different type of plaster, i.e. cementitious and lime-based, considering a plaster with thickness of 3 cm (left) or 5 cm (right). It should be reminded that the cementitious plaster had a mean compressive strength of 33.8 MPa, while the lime plaster 18.9 MPa.

In the case of plaster thickness of 3 cm, the variation in terms of peak loads between cementitious and lime plasters was limited. On the contrary, in the case of 5 cm plaster, the lime mortar allowed a significant increase of the peak load with respect to cementitious one. However, this latter showed a better behaviour after the peak, being able to maintain a certain load for several cycles, after an initial load decrease. In case of lime plaster, the behaviour after the peak resulted more brittle, with a sudden drop of the load. Indeed, at the beginning of the tests, the applied load was distributed over the whole masonry specimen and plaster layers. But, at a certain point, due to the lower plaster strength with respect to the cementitious plaster, the plaster coating was strongly damaged on the corners and the load applied only to the top part of the masonry wall which was also damaged. For this reason, a sudden failure was observed which resulted in a sudden drop of the load. Additionally, the lime plaster always resulted in higher displacement at the peak.

Fig. 11 shows the ultrasonic measurements performed during the execution of the tests at the cycle of 200 % for the cementitious (a) and lime (b) plaster specimens with 3 cm overlay, and at the cycle of 200 % and 150 % for the cementitious (c) and lime (d) plaster specimens with 5 cm overlay. It is evident how, at the same level of applied displacement (or even lower in the case of 5 cm plaster), the damage on the cementitious specimen was more evident, with a large area of detachment of the plaster coating from the masonry (black areas). This extensive damage was observed in lime plaster specimen at higher level of displacement (about cycle 400 %). This phenomenon can be associated to the fact that the lime mortar is a softer material with respect to the cementitious one, with a lower modulus of elasticity and a better compatibility with the masonry substrate. This resulted in a delayed damage propagation and plaster detachment in comparison with the cementitious plaster, and a consequent higher stroke and, in some cases, also higher peak load.

Different failure patterns were detected for the different plaster types. In the case of cementitious plaster, fine multiple cracks were detected on a wide area along the loaded diagonal, with crushing of the plaster at the loaded corners (Fig. 12a). Close to the peak load,

Fig. 8. Damage pattern at the end of the test for specimens MR2-3-8-C-1 and MR2-5-8-C-2.

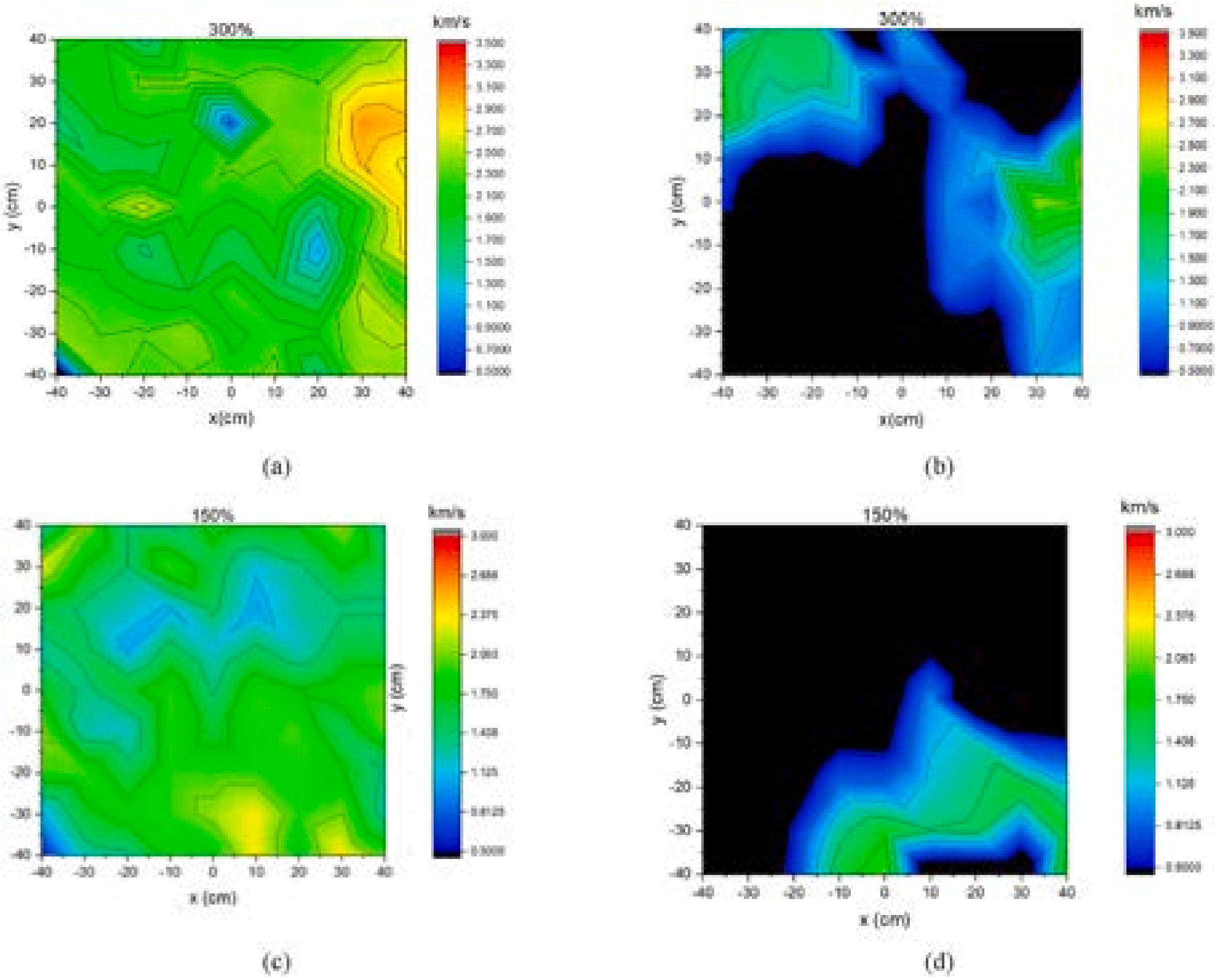

Fig. 9. Ultrasonic measurements for specimens with different plaster thickness: (a) lime plaster with 3 cm thickness (MR2-3-8-L); (b) lime plaster with 5 cm thickness (MR2-5-8-L); (c) cementitious plaster with 3 cm thickness (MR2-3-8-C-1); (d) cementitious plaster with 3 cm thickness (MR2-3-8-C-1).

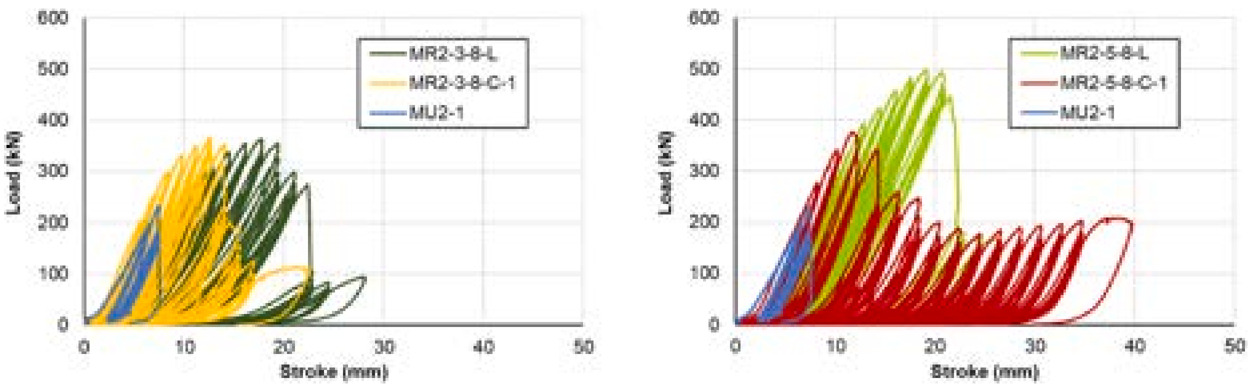

Fig. 10. Load vs. displacement curves for specimens with different type of plaster: left, cementitious and lime plaster with 3 cm of plaster thickness, right, cementitious and lime plaster with 5 cm of plaster thickness.

the plaster cover detached from the substrate (Fig. 12b). In the post peak phase, punching of the plaster was also observed due to the anchors bending. At the end of the test, after the removal of the plaster layer, the masonry resulted interested by multiple cracks, crossing both brick and mortar (Fig. 12c). In case of lime plaster, thin multiple cracks were also detected on a wide area along the

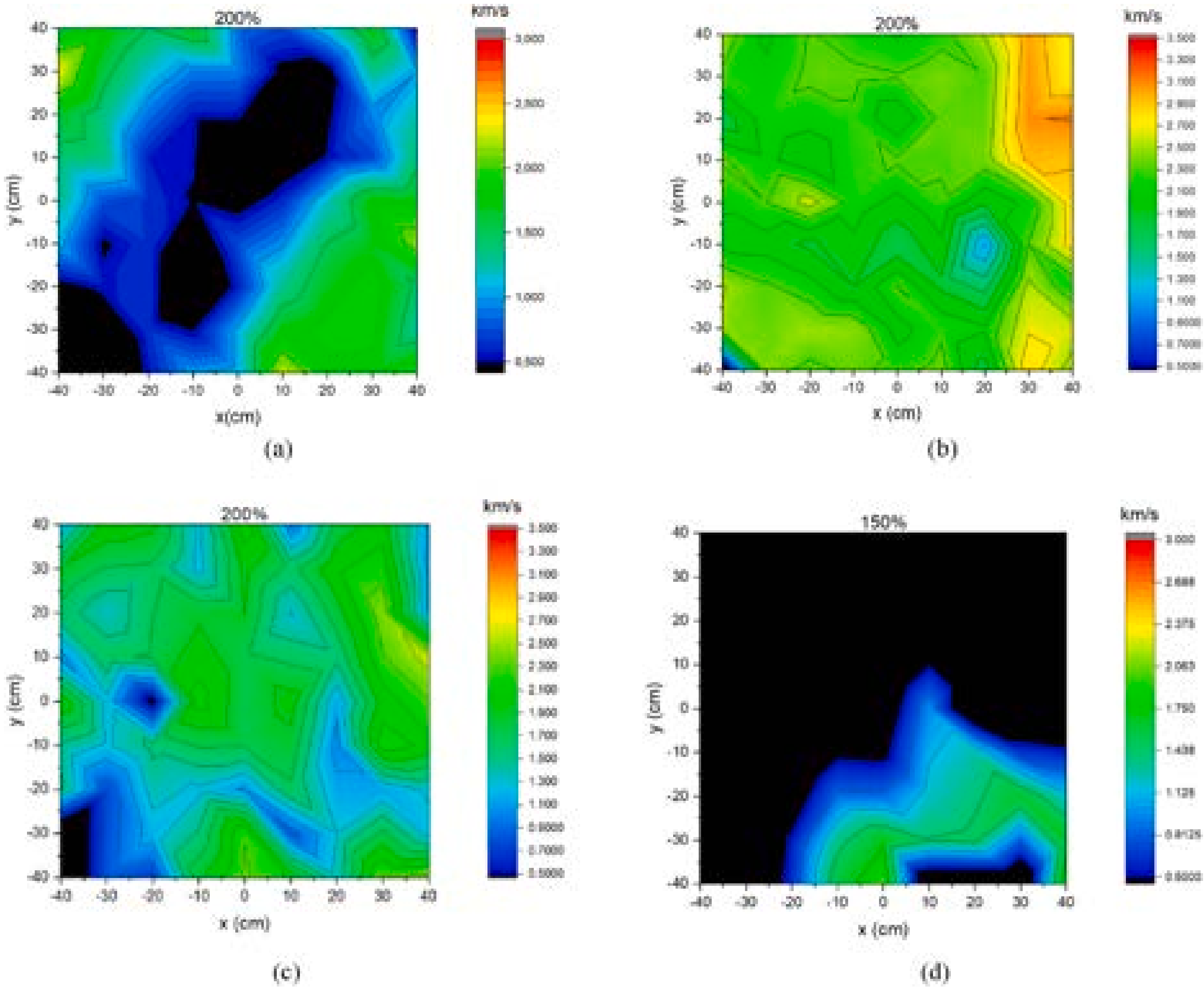

Fig. 11. Ultrasonic measurements for specimens with different type of plaster and different plaster thickness: (a) cementitious plaster (MR2-3-8-C-1) and (b) lime plaster (MR2-3-8-L) at cycle 200 % with plaster thickness 3 cm; (c) cementitious plaster (MR2-5-8-C-1) and (d) lime plaster (MR2-5-8-L) at cycle 200 % and 150 % with plaster thickness 5 cm.

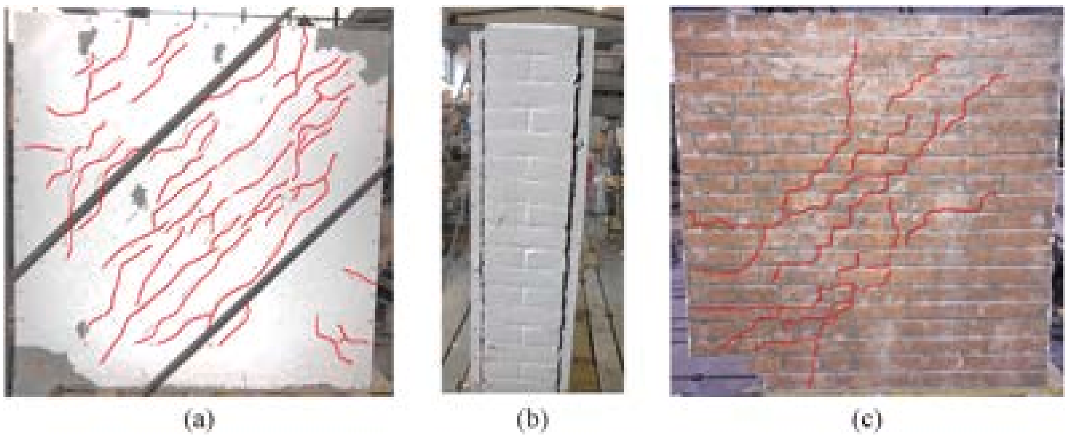

Fig. 12. Damage pattern at the end of the test for cementitious plaster specimen MR2-3-8-C-1: (a) front, (b) side and (c) on masonry behind the plaster.

loaded diagonal (Fig. 13a). The plaster crushing at corners was more evident due to the lower strength of the plaster (Fig. 13b), with significant loss of material (spalling) such that, at a certain point of the test, the load was applied directly to the top part of the masonry wall. Probably for this reason, a sliding of the first 2 or 3 rows of bricks was observed in some of the tests (Fig. 13c). Additionally, the plaster punching was observed only in few cases in the specimens with 3 cm plaster, while it was not observed at all in the case of 5 cm plaster.

3.4. Effect of the number of anchors

Fig. 14 shows the load vs. displacement curves of unreinforced and retrofitted specimens with different number of anchors, i.e. 8 or 12, considering a lime plaster with thickness of 3 cm (left) or 5 cm (right).

In the configurations considered, the number of anchors does not affect significantly the load capacity. However, a stiffness and ductility increase of the structure were detected by increasing the anchors from 8 to 12. Additionally, a higher number of anchors resulted in a late and more controlled detachment of the plaster layers during the tests, with more limited out-of-plane displacements as evident from Fig. 15, in which the out-of-plane displacements recorded on both sides of the specimens (at the top and the bottom) vs. cycles are reported for tests MR2-3-8-L and MR2-3-12-L. Indeed, in the case with 8 anchors, significant out-of-plane displacements were already detected at about 60 cycles, while, in case of 12 anchors, the out-of-plane displacement developed after cycle 75.

4. Analytical evaluations

An analytical approach has been proposed to predict the failure load of masonry walls retrofitted with SRP under diagonal compression test [39]. The method accounts for the main parameters affecting the performance of the strengthened wall such as the masonry properties, the plaster properties and the spacing and number of connectors. The approach has been calibrated using the results of the experimental program conducted on the masonry specimens retrofitted with cementitious mortar plaster [38], and validated using experimental data on similar specimens available in literature [37,39,46]. A further validation will be made in the following considering also the results coming from the experimental program conducted on the masonry specimens retrofitted with lime-based mortar plaster.

The masonry wall is studied as a diagonal strut with length L_d equal to the diagonal length of the wall, and width $w = 0.15L_d$. Two possible failure mechanisms are considered for the reinforced plaster, i.e. crushing and instability of the plaster layer (possible after the plaster detachment from the masonry substrate).

The ultimate load N_{max} is evaluated as the sum of the contribution provided by the masonry and the one given by each plaster layer as:

$$N_{max} = \min\{2N_{p,i} + N_m, 2N_{p,c} + N_m\} \tag{1}$$

where N_m is the maximum load in masonry, while $N_{p,i}$ and $N_{p,c}$ are the maximum load in each plaster layer associated to the instability and crushing failure, respectively.

The masonry strut maximum load N_m is evaluated as:

$$N_m = f_m \cdot w \cdot t_m \tag{2}$$

with f_m masonry compressive strength and t_m masonry thickness.

The limit load $N_{p,c}$ associated with the crushing of the plaster is calculated as:

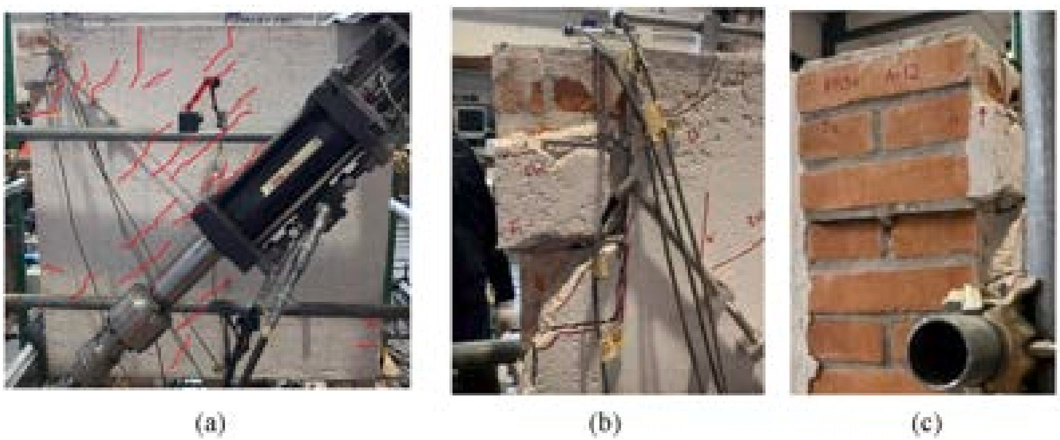

Fig. 13. Damage pattern at the end of the test for lime plaster specimen MR2-3-12-L: (a) front, (b) corner and (c) sliding of the masonry bricks.

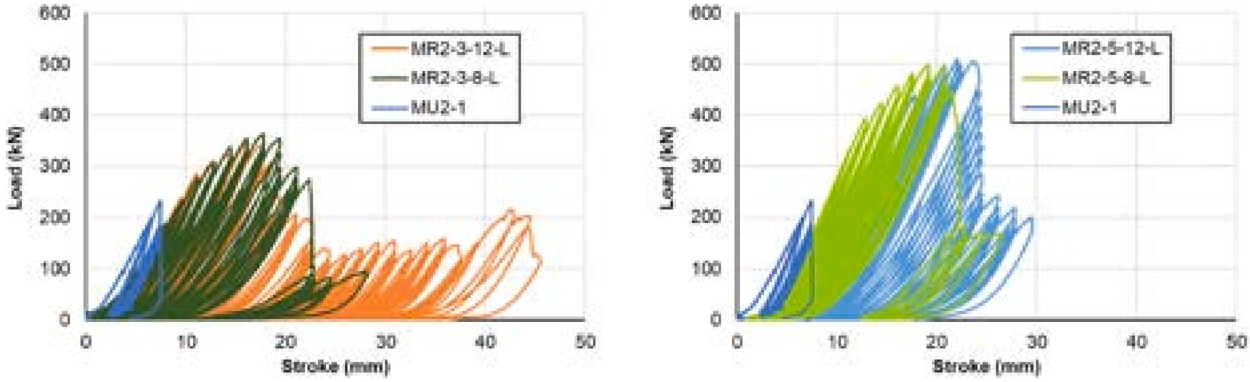

Fig. 14. Load vs. displacement curves for specimens with different number of anchors: left, 3 cm of lime plaster with 8 or 12 anchors, right, 5 cm of lime plaster with 8 or 12 anchors.

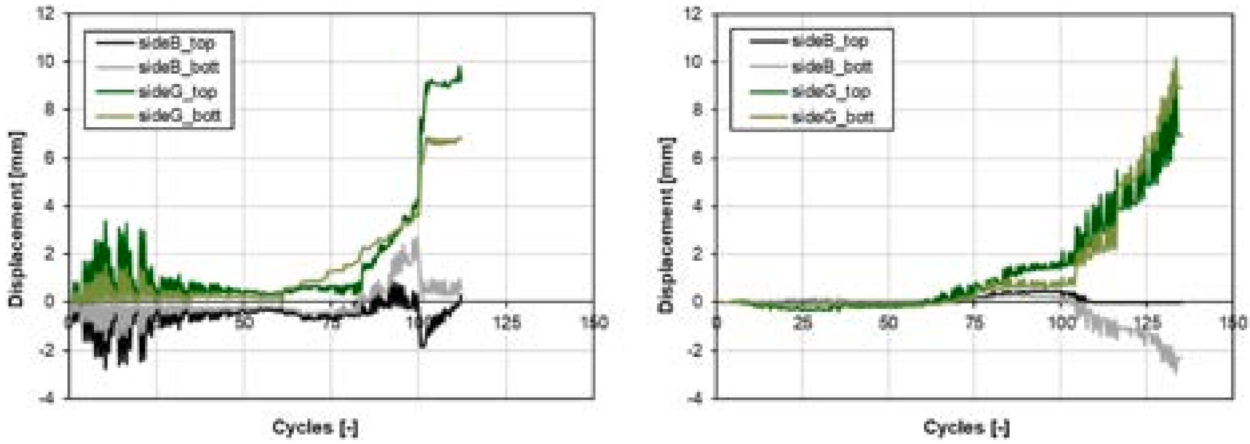

Fig. 15. Displacement vs. cycles curves for specimens with different number of anchors: left, 8 anchors (MR2-3-8-L) and right, 12 anchors (MR2-3-12-L).

$$N_{p,c} = f_{c,r} \cdot w \cdot t_p \tag{3}$$

where t_p is the plaster layer thickness and $f_{c,r}$ is its compressive strength, reduced to take into account the effect of shear cracks on the compressive resistance.

The limit load $N_{p,i}$ associated with the buckling failure of the plaster is calculated as:

$$N_{p,i} = P_e \cdot i \cdot c_{cr} \tag{4}$$

where P_e is the Euler's buckling load of the plaster strut, i is a coefficient to account for the presence of initial imperfections (e.g., construction imperfections, eccentricity of the load), and c_{cr} is a coefficient which accounts for the stiffness and spacing of the connectors. The formulation and all the coefficients have been described in detail in Ref. [39].

Table 3 reports the experimental (P_{exp}) and analytical (N_{max}) ultimate load for comparison, and the required input parameters: L is the side dimension of the masonry specimen, t_m is the wall thickness, f_m is the mean masonry compressive strength, t_p is the plaster thickness, f_c is the mean plaster compressive strength, n is the number of connectors per square meters. In the last column, the percentage change of the analytical result with respect to the experimental one is reported as well. For the evaluation of the masonry compressive strength f_m starting from the compressive strength of brick and mortar (experimentally evaluated), the formulation proposed by Dayaratnam [47] has been adopted, which results suitable for "poor quality" masonry specimens.

When more repetitions of a certain configuration were available, the mean value of P_{exp} is reported. It should be highlighted that the only parameter which depends on the type of plaster (cementitious or lime) is the plaster compressive strength f_c. The results

Table 3
Input parameters, experimental (P_{exp}) and analytical (P_{an}) ultimate loads.

Code	L (mm)	t_m (mm)	f_m (MPa)	t_p (mm)	f_c (MPa)	n (1/m^2)	P_{exp} (kN)	N_{max} (kN)	±%
MU2	1290	250	3.08	–	–	–	198.7	211.0	+6 %
MR3	1290	380	3.08	–	–	–	340.4	320.8	−6 %
MR2-3-8-C	1290	250	3.08	30	33.8	4.8	369.6	356.0	−4 %
MR2-5-8-C	1290	250	3.08	50	33.8	4.8	375.3	508.0	+26 %
MR3-5-8-C	1290	380	3.08	50	33.8	4.8	552.5	617.8	+11 %
MR2-3-8-L	1290	250	3.08	30	18.9	4.8	363.3	340.2	−7 %
MR2-3-12-L	1290	250	3.08	30	18.9	7.21	344.1	354.3	+3 %
MR2-5-8-L	1290	250	3.08	50	18.9	4.8	497.8	475.6	−5 %
MR2-5-12-L	1290	250	3.08	50	18.9	7.21	509.4	505.9	−1 %

coming from the whole experimental program (cementitious and lime plaster) are reported.

The results shows that the analytical model is able to well predict the experimental evidence, also in the case of overlay made of lime mortar plaster. The percentage change related to the test MR2-5-8-C shows the highest error (+26 %). However, this experimental result, which belongs to the masonry specimens of 250 mm thickness, retrofitted with 5 cm of cementitious based plaster, was unexpected and considered as an outlier (see Ref. [38]). Neglecting this value, the percentage change for the retrofitted specimens ranges reasonably between −7 % and +11 %, proving the validity of the approach also in case of lime-based plaster.

Fig. 16 shows the comparison between experimental and predicted values for unreinforced and retrofitted masonry specimens together with the coefficient of determination R^2 and the regression line. A good agreement is evident with a coefficient of determination equal to 0.8283 and a regression line almost coincident to the bisector.

5. Parametric study

The proposed analytical formulation [39] will be used in the following to perform a parametric study for better understanding the sensitivity of the model to some design parameters. It must be underlined that, due to the limited quantity of available experimental data, the results presented in the following could not be always properly validated. However, the calibration and validation procedure discussed in the previous section provided satisfying results, so it seems reasonable to use the method to make some additional interesting considerations.

Among the input parameters required to use the analytical approach, the investigated ones are: (i) the plaster thickness, (ii) the plaster compressive strength, and (iii) the number of anchors. The parameters range has been chosen according to the most common values adopted in the job sites. For the parameters that are not explicit, the input values of test MR2-3-8-L have been adopted (f_m = 3.08 MPa, t_m = 250 mm, f_c = 18.9 MPa, t_p = 30 mm, n = 4.8).

Fig. 17 shows the effect of the plaster thickness on the load capacity of the specimen, considering different compressive strengths f_c of the plaster (left) and different number n of anchors (right). The crosses on the curves represent the point in which the change from one failure mode (crushing) to the other (buckling) or vice versa has been detected. According to Fig. 17, left, for low plaster strength (5 MPa), a linear trend is detected by increasing the plaster thickness with a dominant crushing failure mode. When f_c = 10 MPa, a switch from crushing to buckling is detected at t_p = 25 mm. For higher strength, an exponential trend is detected by increasing the plaster thickness, and the dominant failure mode is the buckling of the overlay. From Fig. 17, right, an almost linear trend is evident with the increasing of the plaster thickness for the different number of anchors. However, in case of n = 3 anchors, the dominant failure

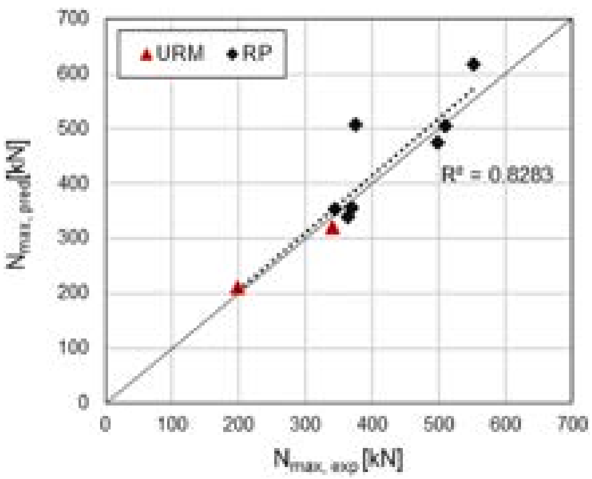

Fig. 16. Experimental and predicted load for unreinforced (URM) and retrofitted (RP) specimens.

mode is the buckling, while, by gradually increase the number of anchors, a change in the failure mode from buckling to crushing is detected for higher plaster thickness. Additionally, for higher plaster thickness and higher number of anchors, the maximum load tends to converge at the same value, i.e. the effect of increasing the number of anchors becomes negligible.

Fig. 18 shows the effect of the number of anchors per square meter on the load capacity of the specimen, considering different compressive strengths f_c of the plaster (left) and different plaster thicknesses (right). The crosses on the curves represent the point in which the change from one failure mode (crushing) to the other (buckling) or vice versa has been detected. According to Fig. 18, left, for low plaster strength (5 MPa), the increase of number of anchors does not affect the load capacity of the specimen, considering that the dominant failure mode is the overlay crushing. By increasing the plaster strength to 10 MPa, for a low number of anchors (up to 3 per square meter), the dominant failure mode is the buckling, which becomes crushing by increasing the number of connectors, keeping constant the maximum load. For higher strength, the dominant failure mechanism is the buckling, so that an increase of the number of connectors n results in an increase of the load capacity, which is however limited, tending to an asymptotic value. In Fig. 18, right, it is evident that the variation of load capacity for increasing number of anchors is limited for lower plaster thickness, in which the buckling is always the dominant failure mode. By increasing the overlay thickness, the variation of load associated to the increasing number of connectors becomes more relevant, even if, when the failure mode changes from buckling to crushing, the load is not affected anymore by the number of anchors ($n = 11$ for $t_p = 40$ mm, $n = 8$ for $t_p = 50$ mm).

In general, the parameters which mainly govern the transition between buckling and crushing are the compressive strength of the plaster and the number of anchors. The crushing failure is usually detected in case of poor compressive strength of the plaster coating (Fig. 17 left, Fig. 18 left). On the other side, an increase of the number of anchors usually corresponds to a change in the failure mode from buckling to crushing. However, for lower number of anchors, higher thicknesses are required to switch from buckling to crushing (Fig. 17 right, Fig. 18 right).

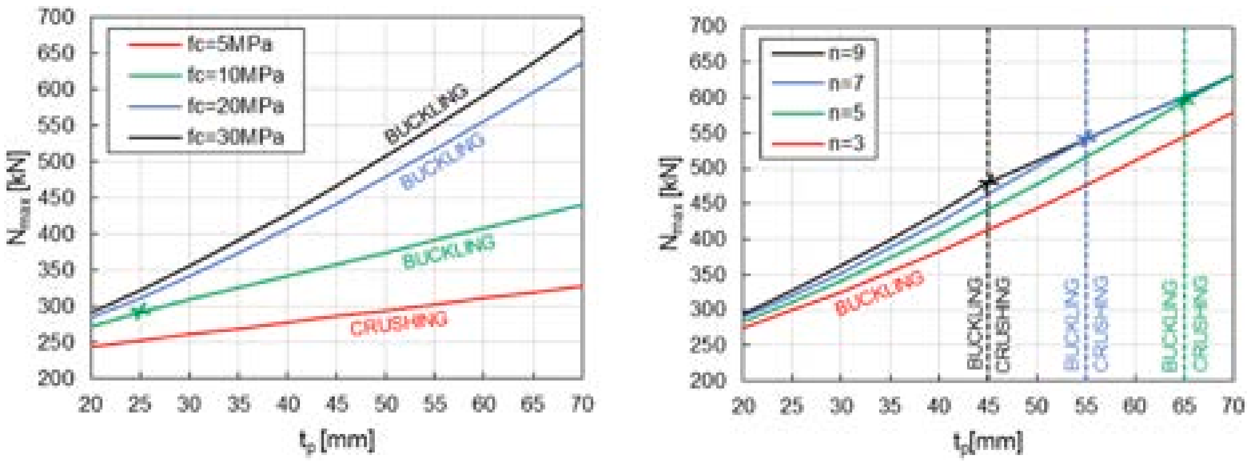

Fig. 17. Effect of the plaster thickness on the maximum load for different compressive strength of the plaster (left) and for different number of anchors (right).

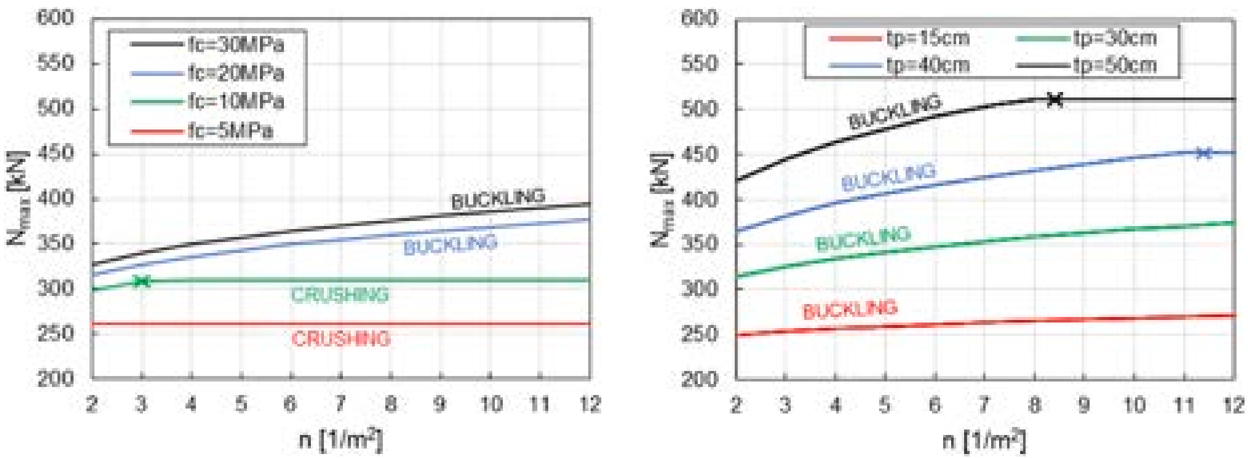

Fig. 18. Effect of the number of anchors per square meter on the maximum load for different compressive strength of the plaster (left) and for different plaster thickness (right).

6. Conclusions

Despite the development of many innovative strengthening techniques in recent years, steel reinforced plaster (SRP) remains one of the most widely used conventional methods for retrofitting unreinforced masonry buildings, due to its cost-effectiveness and substantial performance enhancement. The paper presented and analyzed the findings from an experimental program involving cyclic diagonal tests on masonry specimens strengthened with SRP. Various design parameters were explored in the tested configurations, including masonry and overlay thickness, compressive strength of the plaster, and the number of anchors connecting the steel reinforcement to the masonry. The objective was to evaluate the impact of these parameters on structural performance. An analytical model was also presented and validated against the experimental results. Finally, the model was used to carry out a parametric study, providing deeper insight into the influence of specific design variables. The main outcomes are summarized in the following:

- the increase of overlay thickness did not affect the load bearing capacity in case of cementitious plaster, but considerably improved the specimen ductility; in case of lime plaster, the increase of plaster thickness resulted instead in an increase of the ultimate load, but with similar dissipation capacity;
- the performance of lime plaster, in terms of load bearing capacity, resulted at least equivalent to the cementitious one, and in some cases (5 cm plaster thickness) superior, with higher displacement at the ultimate load and a brittle post peak behaviour; the dissipation capacity (areas of hysteresis loop) of the two types of plaster resulted similar; however, the cementitious plaster was able to maintain a certain load after the peak, while, in the case of the lime one, a sudden drop of the load was usually observed after the peak;
- the number of anchors did not affect significantly the load capacity, but a higher number of anchors resulted in a late detachment of the plaster layers during the tests, with more limited out-of-plane displacements;
- the analytical method previously presented by the authors for the prediction of the load capacity of masonry walls retrofitted with cementitious SRP resulted also valid in case of lime-based plaster;
- the parametric study confirmed that the strength and thickness of the overlay are crucial for the load bearing capacity of the specimen, while the number of connectors does not affect significantly the ultimate load.

It should be remarked that the presented results are related to a small experimental database, with limited variations of the investigated parameters. Therefore, the drawn conclusions should be limited to the studied configurations. Further experiments should be performed to confirm the observed trend and examine in depth the effects of all the design parameters on the masonry performance.

CRediT authorship contribution statement

Manuela Scamardo: Writing – review & editing, Writing – original draft, Visualization, Validation, Software, Methodology, Investigation, Formal analysis, Data curation. **Sara Cattaneo:** Writing – review & editing, Supervision, Resources, Project administration, Methodology, Data curation, Conceptualization. **Pietro Crespi:** Writing – review & editing, Supervision, Methodology, Investigation, Conceptualization.

Declaration of competing interest

The authors declare that they have no known competing financial interests or personal relationships that could have appeared to influence the work reported in this paper.

Acknowledgments

While opinions, findings, and conclusions are those of the authors, we would like to thank Roberto Piccinin, Georg Weltz from Hilti AG and Nicola Viale from Hilti Italia S.p.A. for their insights, expertise and suggestions throughout the preparation and review of this article, together with the technical staff of the Materials and Structures Testing Laboratory of Politecnico di Milano (particularly, Mr. Daniele Spinelli) and Dr. Navid Vafa for their assistance during the experimental work.

Data availability

The data that has been used is confidential.

References

[1] A. Penna, C. Calderini, L. Sorrentino, C.F. Carocci, E. Cescatti, R. Sisti, et al., Damage to churches in the 2016 central Italy earthquakes, Bull. Earthq. Eng. 17 (2019), https://doi.org/10.1007/s10518-019-00594-4.
[2] G. Fiorentino, A. Forte, E. Pagano, F. Sabetta, C. Baggio, D. Lavorato, et al., Damage patterns in the town of Amatrice after August 24th 2016 Central Italy earthquakes, Bull. Earthq. Eng. 16 (2018) 1399–1423, https://doi.org/10.1007/s10518-017-0254-z.
[3] İ. Kocaman, The effect of the Kahramanmaraş earthquakes (Mw 7.7 and Mw 7.6) on historical masonry mosques and minarets, Eng. Fail. Anal. 149 (2023), https://doi.org/10.1016/j.engfailanal.2023.107225.

[4] S. Bhattacharya, S. Nayak, S.C. Dutta, A critical review of retrofitting methods for unreinforced masonry structures, Int. J. Disaster Risk Reduct. 7 (2014) 51–67, https://doi.org/10.1016/j.ijdrr.2013.12.004.
[5] G. Cianchino, M.G. Masciotta, C. Verazzo, G. Brando, An overview of the historical retrofitting interventions on churches in Central Italy, Appl. Sci. 13 (2023), https://doi.org/10.3390/app13010040.
[6] P. Foraboschi, Structural restoration of a historic palace in Italy, Case Stud. Constr. Mater. 22 (2025), https://doi.org/10.1016/j.cscm.2025.e04292.
[7] M.A. Elgawady, P. Lestuzzi, A review of conventional seismic retrofitting techniques for URM, in: 13th International Brick and Block Masonry Conference, 2004, pp. 1–10.
[8] S.R.S. Rezaee, M. Soltani, M. Nikooravesh, Cyclic in-plane behavior of unreinforced and confined masonry walls retrofitted by shotcrete: experimental investigation, Eng. Struct. 264 (2022), https://doi.org/10.1016/j.engstruct.2022.114432.
[9] S. Casacci, C. Gentilini, A. Di Tommaso, D.V. Oliveira, Shear strengthening of masonry wallettes resorting to structural repointing and FRCM composites, Constr. Build. Mater. 206 (2019) 19–34, https://doi.org/10.1016/J.CONBUILDMAT.2019.02.044.
[10] S. Cattaneo, P. Crespi, M. Scamardo, N. Vafa, Cyclic behavior of masonry walls retrofitted with post-installed twisted bars or bonded rebars, Constr. Build. Mater. 409 (2023), https://doi.org/10.1016/j.conbuildmat.2023.134026.
[11] M. Jarc Simonič, S. Gostič, V. Bosiljkov, R. Žarnić, In-situ and laboratory tests of old brick masonry strengthened with FRP in innovative configurations and design considerations, Bull. Earthq. Eng. 13 (2015) 257–278, https://doi.org/10.1007/s10518-014-9644-7.
[12] S. Cattaneo, M. Scamardo, Assessment of the tensile behavior of twisted steel connectors for masonry retrofitting, Constr. Build. Mater. 392 (2023), https://doi.org/10.1016/j.conbuildmat.2023.131771.
[13] F. Ferretti, A. Incerti, A.R. Tilocca, C. Mazzotti, In-plane shear behavior of stone masonry panels strengthened through grout injection and fiber reinforced cementitious matrices, Int. J. Architect. Herit. 15 (2021), https://doi.org/10.1080/15583058.2019.1675803.
[14] M. Buyuktapu, Maras M. Murat, Optimization of production parameters of novel hybrid fiber-reinforced geopolymer mortar: application in masonry walls, Structures 53 (2023), https://doi.org/10.1016/j.istruc.2023.05.031.
[15] S.A. Babatunde, Review of strengthening techniques for masonry using fiber reinforced polymers, Compos. Struct. 161 (2017), https://doi.org/10.1016/j.compstruct.2016.10.132.
[16] M. Taghdi, M. Bruneau, M. Saatcioglu, Seismic retrofitting of low-rise masonry and concrete walls using steel strips, J. Struct. Eng. 126 (2000), https://doi.org/10.1061/(ASCE)0733-9445(2000)126:9(1017).
[17] A.B. Habieb, F.A. Rofiussan, D. Irawan, G. Milani, B. Suswanto, A. Widodo, et al., Seismic retrofitting of Indonesian masonry using bamboo strips: an experimental study, Buildings 13 (2023), https://doi.org/10.3390/buildings13040854.
[18] Z. Zhong, J. Pan, J. Shen, H. Wang, Y. Zhang, X. Du, Experimental study on seismic performance of damaged masonry walls reinforced with high-polymer cementitious composite material, J. Build. Eng. 96 (2024), https://doi.org/10.1016/j.jobe.2024.110629.
[19] M.M. Maras, M.M. Kose, Structural behavior of masonry panels strengthened using geopolymer composites in compression tests, Iran. J. Sci. Technol. Trans. Civ. Eng. 45 (2021), https://doi.org/10.1007/s40996-020-00433-6.
[20] D. Ungureanu, Nicolae Tă, D.A. Ghiga, D.N. Isopescu, P. Mihai, R. Cozmanciuc, Diagonal tensile test on masonry panels strengthened with textile-reinforced mortar. https://doi.org/10.3390/ma14227021, 2021.
[21] J.A.P.P. Almeida, E.B. Pereira, J.A.O. Barros, Assessment of overlay masonry strengthening system under in-plane monotonic and cyclic loading using the diagonal tensile test, Constr. Build. Mater. 94 (2015) 851–865, https://doi.org/10.1016/j.conbuildmat.2015.07.040.
[22] A. Prota, G. Marcari, G. Fabbrocino, G. Manfredi, C. Aldea, Experimental in-plane behavior of tuff masonry strengthened with cementitious matrix–grid composites, J. Compos. Construct. 10 (2006) 223–233, https://doi.org/10.1061/(asce)1090-0268(2006)10:3(223).
[23] A. Hasnat, R. Ahsan, Quasi - static in - plane behavior of full - scale unreinforced masonry walls retrofitted using ferro - cement overlay, Asian J. Civ. Eng. (2022), https://doi.org/10.1007/s42107-022-00447-7.
[24] G. Baloević, J. Radnić, N. Grgić, D. Matešan, The application of a reinforced plaster mortar for seismic strengthening of masonry structures, Compos. B Eng. 93 (2016) 190–202, https://doi.org/10.1016/j.compositesb.2016.03.007.
[25] F. Ceroni, A. Garofano, M. Pecce, Finite Element Modelling of Masonry Panels Reinforced with FRP Grids, 2010.
[26] J.H. Yu, J.H. Park, Compressive and diagonal tension strengths of masonry prisms strengthened with amorphous steel fiber-reinforced mortar overlay, Appl. Sci. 11 (2021), https://doi.org/10.3390/APP11135974.
[27] Y.W. Lin, L. Wotherspoon, A. Scott, J.M. Ingham, In-plane strengthening of clay brick unreinforced masonry wallettes using ECC shotcrete, Eng. Struct. 66 (2014) 57–65, https://doi.org/10.1016/j.engstruct.2014.01.043.
[28] Ministero delle infrastrutture e dei Trasporti, Decreto Ministeriale 17 Gennaio 2018 C.S.LL.PP. Aggiornamento delle «Norme tecniche per le costruzioni», 2018.
[29] Ministero delle Infrastrutture e dei Trasporti, Circolare 21 gennaio 2019, n. 7 C.S.LL.PP. Istruzioni per l'applicazione dell'«Aggiornamento delle Norme tecniche per le costruzioni», 2019, pp. 1–14.
[30] Eartquake planning and protection organization (E.E.P.O, KAN.EPE. Code of interventions on reinforced concrete buildings, in: English Version after Harmonization with Eurocode 8, Part 3, 2013, pp. 1–337.
[31] Federal Emergency Management Agency, American society of civil engineers, in: FEMA 356 Prestandard and Commentary for the Seismic Rehabilitation of Buildings, 2000.
[32] Z. Chen, H. Liu, L. Xu, W. Ge, A review of mechanical properties and carbonation behavior evolution of lime mortar for architectural heritages restoration, Miner. Miner. Mater. 3 (2024), https://doi.org/10.20517/mmm.2023.26.
[33] M. Scamardo, S. Cattaneo, P. Crespi, Assessment of reinforced overlay for masonry retrofitting: lime vs cementitious plaster, in: MATEC Web of Conferences, 403, 2024 07001, https://doi.org/10.1051/matecconf/202440307001.
[34] B. Ghiassi, M. Soltani, A.A. Tasnimi, Seismic evaluation of masonry structures strengthened with reinforced concrete layers. https://doi.org/10.1061/(ASCE)ST.1943-541X, 2012.
[35] S. Churilov, E. Dumova-Jovanoska, In-plane shear behaviour of unreinforced and jacketed brick masonry walls, Soil Dynam. Earthq. Eng. 50 (2013) 85–105, https://doi.org/10.1016/j.soildyn.2013.03.006.
[36] N. Gattesco, I. Boem, A. Dudine, Diagonal compression tests on masonry walls strengthened with a GFRP mesh reinforced mortar coating, Bull. Earthq. Eng. 13 (2015) 1703–1726, https://doi.org/10.1007/s10518-014-9684-z.
[37] G. Maddaloni, Analisi sperimentale del comportamento di edifici in muratura rinforzati con tecniche e materiali innovativi, 2017.
[38] L. Biolzi, S. Cattaneo, P. Crespi, M. Scamardo, N. Vafa, Diagonal compression cyclic testing of unreinforced and reinforced masonry walls, Constr. Build. Mater. 363 (2023).
[39] M. Scamardo, S. Cattaneo, P. Crespi, L. Biolzi, Design method for masonry structures retrofitted with steel reinforced plaster, J. Build. Eng. 79 (2023), https://doi.org/10.1016/j.jobe.2023.107828.
[40] European Committee for Standardization, EN 1996-1-1 Eurocode 6 - Design of Masonry Structures - Part 1-1: General Rules for Reinforced and Unreinforced Masonry Structures Eurocode, 2005.
[41] ASTM C67/C67M-21, Standard Test Methods for Sampling and Testing Brick and Structural Clay Tile, ASTM International, 2021.
[42] ASTM C109/C109M-02, Standard test method for compressive strength of hydraulic cement mortars, Annu. Book ASTM (Am. Soc. Test. Mater.) Stand. 4 (2020).
[43] ASTM C348-21, Standard test method for flexural strength of hydraulic-cement mortars, Annu. Book ASTM (Am. Soc. Test. Mater.) Stand. (2021).
[44] ASTM International, Astm E519 - standard test method for diagonal tension (shear) in masonry assemblages. https://doi.org/10.1520/E0519, 2021.
[45] M.L. Porter, Sequential phased displacement (SPD) procedure for TCCMAR testing, in: Third Meeting of the Joint Technical Coordinating Committee on Masonry Research, U.S. - Japan Coordinated Earthquake Research Program, Tomamu, Japan, 1987.
[46] N. Gattesco, I. Boem, Experimental and analytical study to evaluate the effectiveness of an in-plane reinforcement for masonry walls using GFRP meshes, Constr. Build. Mater. 88 (2015) 94–104, https://doi.org/10.1016/J.CONBUILDMAT.2015.04.014.
[47] P. Dayaratnam, Brick and Reinforced Brick Structures, Oxford & IBH, 1987.